



Universiteit
Leiden
The Netherlands

Frequency conversion in two-dimensional photonic structure

Babic, L.

Citation

Babic, L. (2011, May 17). *Frequency conversion in two-dimensional photonic structure*. *Casimir PhD Series*. Retrieved from <https://hdl.handle.net/1887/17642>

Version: Not Applicable (or Unknown)

License: [Leiden University Non-exclusive license](#)

Downloaded from: <https://hdl.handle.net/1887/17642>

Note: To cite this publication please use the final published version (if applicable).

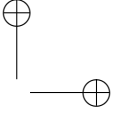

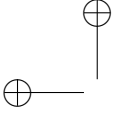
CHAPTER 4

Method to transfer photonic crystals to a transparent gel substrate

4.1 Introduction

Over the last two decades, the continuous expansion of the field of photonic crystals went hand in hand with developments in semiconductor nanofabrication techniques. Since the introduction of photonic crystals as structures that can form a complete band gap to inhibit spontaneous emission [5], or localize light [6], many novel properties of these fascinating materials have been found and experimentally realized. Today, photonic crystals are recognized as structures that offer remarkable control of light propagation and enhanced light-matter interaction. As such, they find applications in lasers, single photon emitters, waveguides, filters, optical nonlinear devices, sensors, and slow light media [9–11]. So far, combining various devices into a single chip has proven to be a very difficult task, since it requires different materials and fabrication techniques.

In this chapter we propose a novel technique to transfer a semiconductor based photonic crystal device to any substrate. The main idea is to stick the structure to a transparent gel film. This gel can then be glued to the desired substrate. If needed, the substrate can have additional patterning in order to add functionality to the system. In contrast to wafer bonding techniques, a dedicated machine is not needed and the interfaces do not have to be polished to an optical quality. This may significantly reduce the time and resources needed to fabricate the desired structure, which is extremely important in the early stage of prototype development where trial and error are often used as



4. Method to transfer photonic crystals to a transparent gel substrate

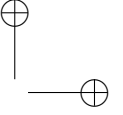
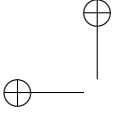
an approach to solve the fabrication issues.

The proposed technique can be used for optical frequency converters based on photonic crystal slabs in III-V semiconductor materials that possess high second-order nonlinearity such as GaN, GaP, or $\text{Al}_x\text{Ga}_{1-x}\text{As}$. Current III-V technology allows epitaxial growth of nearly lattice matched AlGaAs layers on GaAs. For a freestanding membrane with a large surface area, the lattice mismatch between the membrane layer and the substrate causes buckling of the membrane. The buckling leads to lower optical quality of the structure. This issue can be overcome by transferring the freestanding membrane to a transparent gel substrate to release the strain.

We have successfully transferred large freestanding $\text{Al}_{0.35}\text{Ga}_{0.65}\text{As}$ photonic crystal membranes ($\sim 300 \times 300 \mu\text{m}^2$) to a transparent gel substrate with a low refractive index of $n_{\text{gel}} = 1.4$. In contrast to the freestanding structure, the membrane on gel is almost flat and the transparent substrate enables transmission measurements. The introduction of the low index substrate results in a red shift of the frequencies of the leaky modes. A simplified coupled mode theory based on a truncated plane wave method [68] in two-dimensions is used to describe an avoided crossing between three modes in our system. Due to the interaction, one of the modes becomes subradiant and reaches Q values of 300, limited by the finite size of our membrane, which demonstrates the excellent optical quality of our structures.

Compared to a similar system patterned in silicon nitride [69], our structures are mechanically more robust and they have a larger index contrast. Therefore, ultrahigh- Q nanocavities in $\text{Al}_{0.35}\text{Ga}_{0.65}\text{As}$ that are transferred to the gel might provide a more promising platform for biochemical sensing in liquid phase [70] than those in silicon nitride membranes. For comparison, a silicon nitride device immersed in water has an index contrast of 1.71 at a wavelength of 780 nm [69], while an index contrast of ≥ 2 is needed to create a band gap for the guided modes [71–73]. The index contrast for the $\text{Al}_{0.35}\text{Ga}_{0.65}\text{As}$ membrane in water is 2.56, and for the $\text{Al}_{0.35}\text{Ga}_{0.65}\text{As}$ membrane on the gel substrate is 2.44, at a wavelength of 780 nm [62]. Both of them exceed what is possible with silicon nitride and the contrast is large enough to create a complete band gap. This enables defect cavities with a high quality factor and a small modal volume for sensing applications.

Another possible application of our technique would be to provide high extraction efficiency for light-emitting diodes (LEDs). In this application a photonic crystal layer with a large index contrast is placed on top of an LED [74] using our transfer technique. Without a photonic crystal layer, the light that is not emitted in the extraction cone is guided in the cladding material. If

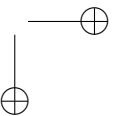
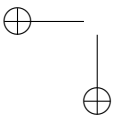


not collected from the edges of the structure, the guided modes are lost. By adding a photonic crystal layer with properly chosen parameters, it becomes possible to diffract large part of guided light into the extraction cone. The advantage of our method is that this layer can be made independently in a separate fabrication stage using a completely different technology. By using the large index contrast of the photonic crystal, a much more strongly diffracting layer is created when compared to existing structures with a small periodic surface corrugations [74].

Our technique could be used to position a gallium phosphide (GaP) membrane with a cavity on a flat diamond substrate with nitrogen-vacancy centers (N-V centers) as an alternative to using a nanodiamond with a single N-V center [75]. These N-V centers in bulk diamond can be isotropically pure and can be positioned using ion implantation [76]. Moreover, such N-V centers have low decoherence [77, 78] which may be important for future applications in quantum information.

4.2 Sample preparation

We fabricated two-dimensional photonic crystal slabs with a square lattice of holes with a hole radius of ~ 150 nm and a lattice constant $a = 820$ nm using a combination of e-beam lithography and reactive ion etching techniques in a commercially grown AlGaAs layer structure [51]. The samples were fabricated using the facilities of the Kavli Nanolab Delft. An overview of the fabrication process is shown in Figure 4.1. The layers in this study are deposited using a MOCVD (metalorganic chemical vapor deposition) process on a $\langle 100 \rangle$ GaAs substrate and consist of a $1 \mu\text{m}$ thick Al rich $\text{Al}_{0.7}\text{Ga}_{0.3}\text{As}$ layer, a 150 nm thick Ga rich $\text{Al}_{0.35}\text{Ga}_{0.65}\text{As}$ layer, and a 100 nm thick GaAs capping layer. To create the hole pattern, a 150 nm silicon nitride layer is deposited on top of the structure and serves as a mask during the final reactive ion etching step. The lattice of holes is created by e-beam lithography in a ~ 500 nm thick layer of positive tone e-beam resist, ZEP 520A [52], as shown in Figure 4.1(a). A low pressure reactive ion etching step in a CHF_3/Ar plasma is used to transfer the hole pattern into the nitride mask. After removal of the e-beam resist in a low pressure O_2 plasma, the hole pattern is etched deep into the AlGaAs heterostructure in a $\text{BCl}_2/\text{Cl}_2/\text{N}_2$ reactive ion etch process at 100 W RF power, a pressure of $\sim 4.5 \mu\text{bar}$ and flow rates of 15 , 7.5 , and 10 sccm respectively. The nitrogen flow in this process was optimized to create near vertical side walls of the holes. After etching the holes, the nitride mask is removed using the CHF_3/Ar etching procedure described above.



4. Method to transfer photonic crystals to a transparent gel substrate

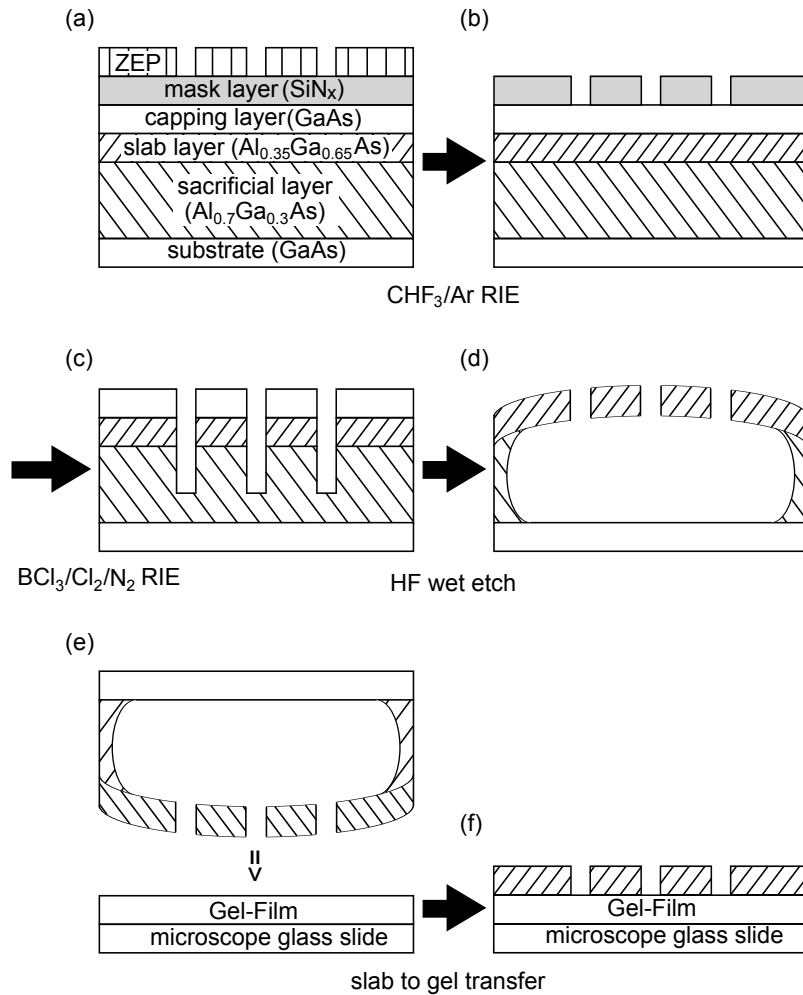


Figure 4.1. Overview of the fabrication process of a photonic crystal slab: (a)-(c) A regular two-dimensional square lattice of holes is created in the AlGaAs/GaAs heterostructure by using e-beam lithography and reactive ion etching. (d) Wet etching techniques are employed to remove both the capping and the sacrificial layer, creating a freestanding photonic crystal slab in air. Due to a small lattice mismatch between the GaAs substrate and the $\text{Al}_{0.35}\text{Ga}_{0.65}\text{As}$ layer, the slab buckles. (e) The photonic crystal slab is then transferred to a gel substrate fixed onto a microscope glass slide. (f) The resulting structure is an almost flat membrane on a transparent substrate (gel) with a low refractive index $n_{gel} = 1.4$.

To create a freestanding membrane we first remove any residual oxide layer by dipping the sample in 15:1 deionized H_2O :buffered hydrofluoric acid (BHF) solution for 15 sec. The sample is then placed in a 3:1 citric acid: H_2O_2 solution for 120 sec to selectively remove the GaAs capping layer. Finally, the freestanding membrane is created by etching the sacrificial $\text{Al}_{0.7}\text{Ga}_{0.3}\text{As}$ layer in a concentrated 1:4 HF (40%): H_2O solution for 60 sec followed by a rinsing step in pure water and critical point drying. The resulting membrane covers an area of $\sim 300 \times 300 \mu\text{m}^2$ and is not perfectly flat due to a small lattice mismatch between the $\text{Al}_{0.35}\text{Ga}_{0.65}\text{As}$ ($l = 0.565603 \text{ nm}$) membrane layer and the GaAs ($l = 0.565325 \text{ nm}$) substrate [79]. This lattice mismatch of about 0.05% causes a compressive strain in the membrane. After etching the sacrificial layer, the freestanding photonic crystal slab buckles releasing the strain. The buckled membrane is symbolically depicted in a form of a bent slab in Figure 4.1(d).

In the end, the membrane is transferred to a transparent gel layer [80] with a refractive index of 1.4 on a standard microscope slide. The sample is gently placed on the gel using tweezers, and the GaAs substrate is carefully peeled off. As a result, an almost flat photonic crystal slab is created, as shown in Figure 4.1(f).

Figures 4.2(a) and (b) show the optical images of a photonic crystal slab before and after the transfer, respectively. As can be seen, a few cracks occur along the sample surface depending on how gently the slab is placed on the gel. Typically, there is a damage free area on the sample that is larger than $\sim 200 \times 200 \mu\text{m}^2$. In addition to the structures with the lattice constant $a = 820 \text{ nm}$, the hole radius $r \sim 150 \text{ nm}$, and the area $A \sim 300 \times 300 \mu\text{m}^2$, we have transferred samples with $a = 960 \text{ nm}$, $r \sim 270 \text{ nm}$, and a surface area $A \sim 425 \times 425 \mu\text{m}^2$, and samples with $a = 350 \text{ nm}$, $r \sim 100 \text{ nm}$, and $A \sim 425 \times 425 \mu\text{m}^2$. Out of about 25 transferred membranes, only about 5 had significant damage or folds from the transfer process. Considering that in those ~ 5 cases the transfer was not done very carefully, we conclude that the $\sim 80\%$ yield can be increased by taking more care during the transfer process. Equally important, membranes that have collapsed onto the substrate during the fabrication process, can be picked up with the gel layer and used in experiments. This demonstrates the robustness and versatility of our technique, and suggests that samples could be made without the use of critical point drying.

Figures 4.2(c) and (d) show the interference microscope images of the slab at a wavelength of 549 nm, before (c) and after (d) the transfer, demonstrating that the structure on the gel is flatter. The equidistant fringes next to the sample in Figure 4.2(c) result from a small angle between the glass slide and

4. Method to transfer photonic crystals to a transparent gel substrate

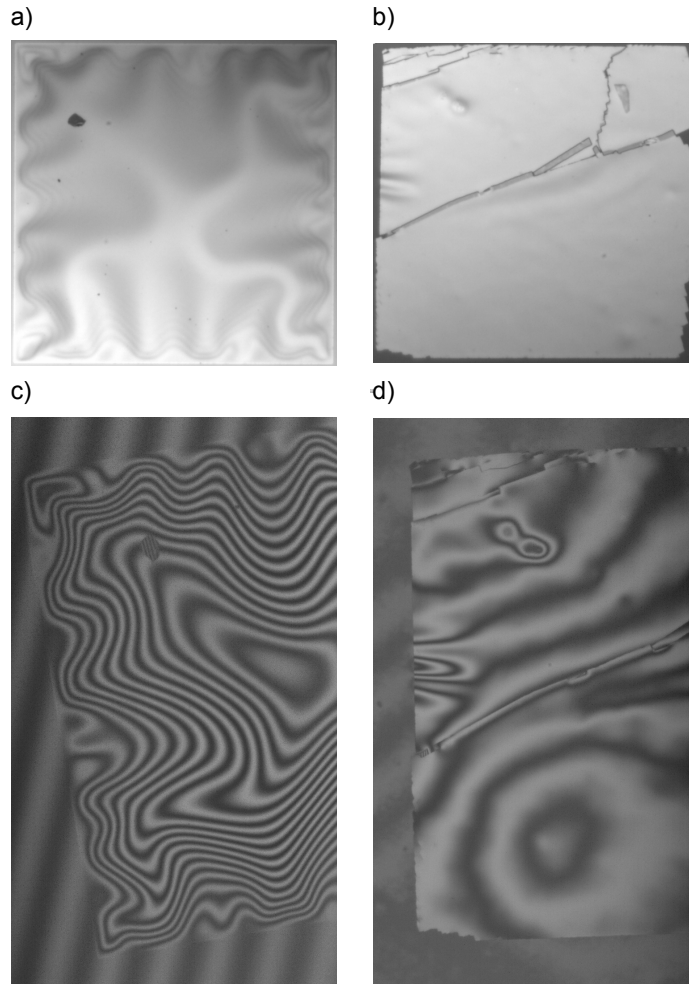
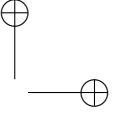
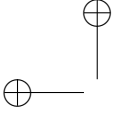


Figure 4.2. Optical microscope images of a freestanding photonic crystal slab (a) and the same photonic crystal slab after being transferred to the gel substrate (b). The sample size is $\sim 300 \times 300 \mu\text{m}^2$. Interference microscope images of the photonic crystal slab before (c) and after (d) placement on the gel showing that the structure on the gel is flatter. The height difference between a neighboring dark and white fringe is 274.5 nm.



the holder of the microscope. To estimate an upper limit for height differences along a membrane before and after the transfer, we count the fringes along the sample diagonal from the edge to the center of the structure. For a typical sample, we estimate the maximum height difference to be $\sim 10 \mu\text{m}$ for a freestanding membrane and $\sim 1 \mu\text{m}$ for a membrane on a gel. This shows that the membranes not only survive the transfer, but also become significantly flatter.

4.3 Experiment

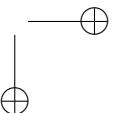
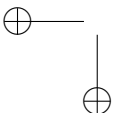
We perform reflection and transmission measurements for wavelengths between 650 and 1700 nm using white light from a lamp coupled to a $50 \mu\text{m}$ multimode fiber. The output of this fiber is imaged onto the sample with a 1.5 times magnification to create a $75 \mu\text{m}$ spot on the sample. Apertures in the beam limit the numerical aperture of the incident beam to $\text{NA} \sim 0.025$. The reflected/transmitted light is collected into a $400 \mu\text{m}$ fiber and then sent to a fiber-coupled grating spectrometer. A silicon CCD array spectrometer (Ocean Optics USB2000) with a spectral resolution of $\approx 1.5 \text{ nm}$ is used for detection in the visible and near-infrared part of the spectrum ($\lambda \sim 650\text{--}900 \text{ nm}$). For the infrared part of the spectrum ($\lambda \sim 900\text{--}1700 \text{ nm}$), we use an InGaAs array spectrometer (Ocean Optics NIR512) with a $\approx 3 \text{ nm}$ spectral resolution. A Glan-Thompson polarizing beamsplitter cube is placed in a parallel part of the beam and is used to measure the reflectivity and transmissivity for s - and p -polarized light as a function of wavelength and angle of incidence.

The experimental setup for measuring the linear reflection spectra is identical to the setup shown in Figure 3.4(a) of Chapter 3. The linear transmission spectra are measured by aligning lenses L3 and L4 to collect the transmitted light rather than the reflected light.

4.4 Results and Discussion

4.4.1 Leaky modes of photonic crystal slabs before and after the transfer to the gel substrate

Figure 4.3 shows typical experimental reflection spectra of a photonic crystal slab before (blue circles) and after (red circles) the transfer to the gel. The measurements are done with p -polarized light incident at an angle of 35° along the ΓX symmetry direction of the square lattice. The reflection spectra consist of sharp resonant features superimposed on a slowly oscillating background.



4. Method to transfer photonic crystals to a transparent gel substrate

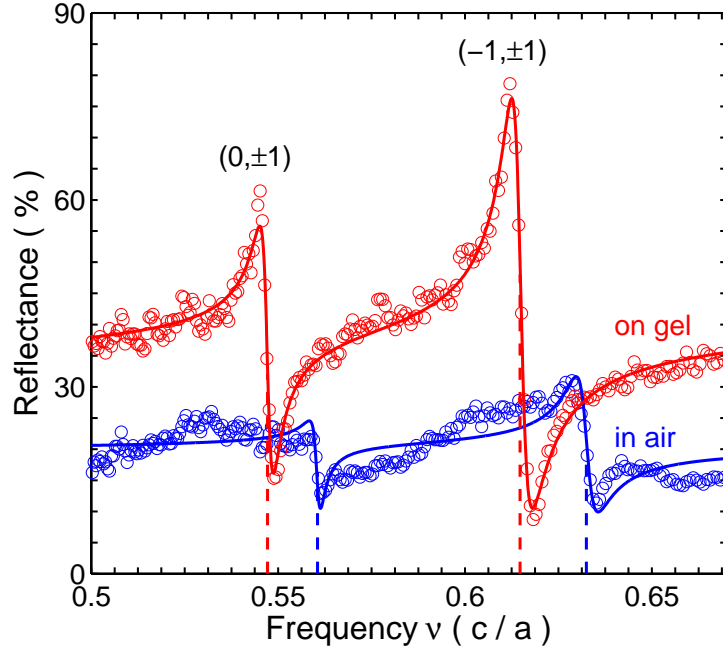


Figure 4.3. Measured reflection spectra of the slab suspended in air (blue circles) and transferred on the gel (red circles). The solid lines are obtained by fitting a Fano model (described in the text) to the experimental data. The dashed lines indicate the center frequencies of the p -polarized $(0, \pm 1)$ and $(-1, \pm 1)$ modes, as determined from the fit.

The two resonances in the spectra are the p -polarized $(0, \pm 1)$ and $(-1, \pm 1)$ leaky modes. A red shift of the resonances is observed after the transfer to the gel. Each leaky mode is labeled by the dimensionless reciprocal lattice vector (G_x, G_y) that is involved in the coupling of the incoming light to the leaky mode. This notation assumes that the plane of the periodicity is parallel to the xy -plane of the Cartesian coordinate system, with the ΓX symmetry direction of the square lattice parallel to the x -axis. Furthermore, we consider an experimental geometry in which the component of the incoming wave vector along the z -axis is perpendicular to the sample, and is denoted as \mathbf{k}_\perp . The component of the incoming wave vector in the xy -plane is labeled as \mathbf{k}_\parallel .

It is clear from the measured spectra that the resonant features for the membrane on the gel substrate are more prominent than those for the freestanding membrane. The main reason for this is the removal of the highly-reflective GaAs substrate. In the case of the freestanding structure, the GaAs

substrate and the membrane act as two mirrors and form a Fabry-Perot cavity with air in between. The observed waviness of the membrane introduces variations in the distance between the substrate and membrane, which are much larger than $\lambda/4$. This creates strong variations in the reflected amplitude of the non-resonant contribution. Illuminating with a large spot is equivalent to averaging over all the substrate to membrane distances, and as a consequence the resonances in the reflection spectra for the freestanding slab have lower visibility compared to the slab transferred to the gel.

To quantify the red shift of the resonances due to the transfer to the gel we fit a Fano model to the measured reflectivity spectra (solid lines in Fig. 4.3). Within this model, the reflectivity as a function of the frequency, $R(\nu)$, is given by [60, 67]

$$R(\nu) = \left| r_D + \sum_j \frac{r_{Rj}}{i(\nu - \nu_j) + \gamma_j + \Gamma_j} \right|^2, \quad (4.1)$$

where r_D represents the non-resonant (direct) contribution, and the sum represents the resonant contribution. Leaky mode j has an amplitude r_{Rj} , a center frequency ν_j , and an escape rate Γ_j . The loss rate γ_j in the model describes losses due to the absorption, higher order diffraction, and the scattering from imperfections of the structure [67]. Accordingly, the quality factor (Q_j) of the leaky mode is defined as $Q_j = \nu_j/(2(\Gamma_j + \gamma_j))$, and can be interpreted as the number of optical periods before the intensity of the mode decays by $e^{-2\pi}$ [68]. To fit experimental data, we assume that the amplitude of the direct contribution, in a small frequency region around the center frequency, can be approximated with a linear function of the frequency ν : $r_D = c_1 + c_2\nu$, and we allow the amplitude r_{Rj} to be a complex number.

From the fits to the measured data in Fig. 4.3 we find frequencies ν_j of 0.561 and $0.633 \times c/a$ for the freestanding structure, and 0.547 and $0.615 \times c/a$ for the structure transferred to the gel. This corresponds to a red shift of 2.5 and 2.8% for the $(0, \pm 1)$ and $(-1, \pm 1)$ mode. Qualitatively this red shift can be understood from a nearly free photon picture [69, 81, 82]. The leaky modes are due to the folded mode of the slab waveguide with an effective refractive index. When the slab is placed on a substrate with a higher refractive index, i.e., gel instead of air, this effective refractive index increases and a red shift is observed.

Although this waveguide model explains the physical origin of the frequency shift, it cannot be used directly for a quantitative description of the experimental data. The waveguide model does not contain a simple way to calculate the effect of the holes on the effective refractive index and does not take

4. Method to transfer photonic crystals to a transparent gel substrate

into account the interaction between the modes. This issue can be resolved by comparing our experimental data with finite-difference time-domain (FDTD) calculations. We use a freely available software package called MEEP [61] to calculate the frequencies of the resonances for an infinite slab with parameters identical to the experimental structure. The calculations are performed for a structure with a lattice constant $a = 820$ nm, a radius of holes $r = 160$ nm, and a thickness of the slab $d = 122$ nm. For the refractive index of the slab material we use a value of 3.1975, which is the tabulated value for the refractive index of the $\text{Al}_{0.35}\text{Ga}_{0.65}\text{As}$ at a wavelength of $1.5 \mu\text{m}$ [62]. The refractive index of the gel is taken to be 1.4. Figure 4.4 shows the measured and the calculated dispersion relations for both the s - and p -polarized $(0, \pm 1)$ modes, for a freestanding membrane and a membrane on the gel. The experimental

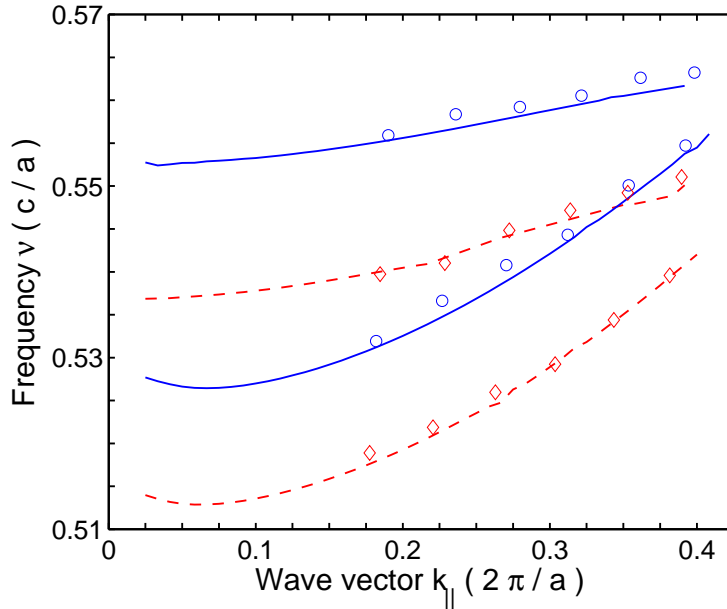


Figure 4.4. Measured (blue circles) and calculated (solid blue lines) dispersion relations of the two $(0, \pm 1)$ modes, for a freestanding membrane. The s -polarized mode is lower in frequency than the p -polarized mode. Measured (red diamonds) and calculated (dashed red lines) dispersion relations of the two $(0, \pm 1)$ modes, for the membrane transferred to the gel substrate. The calculations are performed for a structure with a lattice constant $a = 820$ nm, a radius of holes $r = 160$ nm, and a thickness of the slab $d = 122$ nm. The refractive indices of the slab material and the gel are taken to be 3.1975 and 1.4, respectively.

dispersion is obtained by fitting a Fano model of Equation 4.1 to the measured reflection spectra done at oblique angles of incidence with the wave vector k_{\parallel} along the ΓX symmetry direction of the square lattice. The s -polarized $(0, \pm 1)$ mode has a lower frequency than the p -polarized $(0, \pm 1)$ mode. As can be seen, the experimental data before (blue circles) and after (red diamonds) the transfer to the gel substrate agree very well with the calculated data for a slab in air (solid blue lines) and a slab with gel instead of air on one of the sides (dashed red lines), and shows a red shift of $\approx 2.5\%$ for the entire band. This uniform shift is consistent with the simple waveguide picture, where the presence of the gel increases the effective refractive index of the slab by $\approx 2.5\%$.

4.4.2 Interaction between the leaky modes of photonic crystal slabs transferred to a gel substrate

Transferring photonic crystal membranes to an optically transparent gel substrate creates flat structures that are ideally suited for transmission measurements. Figure 4.5 shows the measured transmission as a function of frequency (vertical axis) and wave vector k_{\parallel} (horizontal axis). Experimental data is shown for both s - (a) and p -polarized (b) light along the ΓX and the ΓM symmetry direction of the square lattice. The transmission spectra reveal many leaky modes also for higher order photonic bands. This demonstrates the excellent optical quality of the transferred structure. In this chapter we will limit the discussion to the lower frequency modes. For s -polarized light with k_{\parallel} along the ΓX symmetry direction, going from low to high frequencies, we observe the $(-1, 0)$, the $(0, \pm 1)$, the $(1, 0)$, and the $(-1, \pm 1)$ leaky modes of the fundamental TE waveguide mode. For frequencies around $\sim 0.7 \times c/a$, we identify the $(0, \pm 1)$ leaky mode of the fundamental TM mode close to the Γ -point. The TM mode interacts with the TE mode [82]. This TE-TM mixing together with higher order waveguide modes complicates the labeling of the modes for frequencies above $0.7 \times c/a$.

We will analyze the interaction between the $(1, 0)$ and $(-1, \pm 1)$ leaky modes of the fundamental TE waveguide mode in detail. For a wave vector k_{\parallel} along the ΓX symmetry direction, the $(1, 0)$ mode couples to s -polarized radiation. Of the two $(-1, \pm 1)$ modes, the low frequency mode couples to s -polarization, while the higher frequency mode couples to p -polarized radiation.

Figure 4.6 shows the measured transmission spectra for angles of incidence from 10° to 40° in steps of 1° (solid gray lines). The curves are vertically offset for clarity. We show the experimental data for the in-plane wave vector k_{\parallel} along the ΓX symmetry direction of the square lattice, for s - (a) and p -polarized (b) light. The data in Figure 4.6(a) shows a clear avoided crossing

4. Method to transfer photonic crystals to a transparent gel substrate

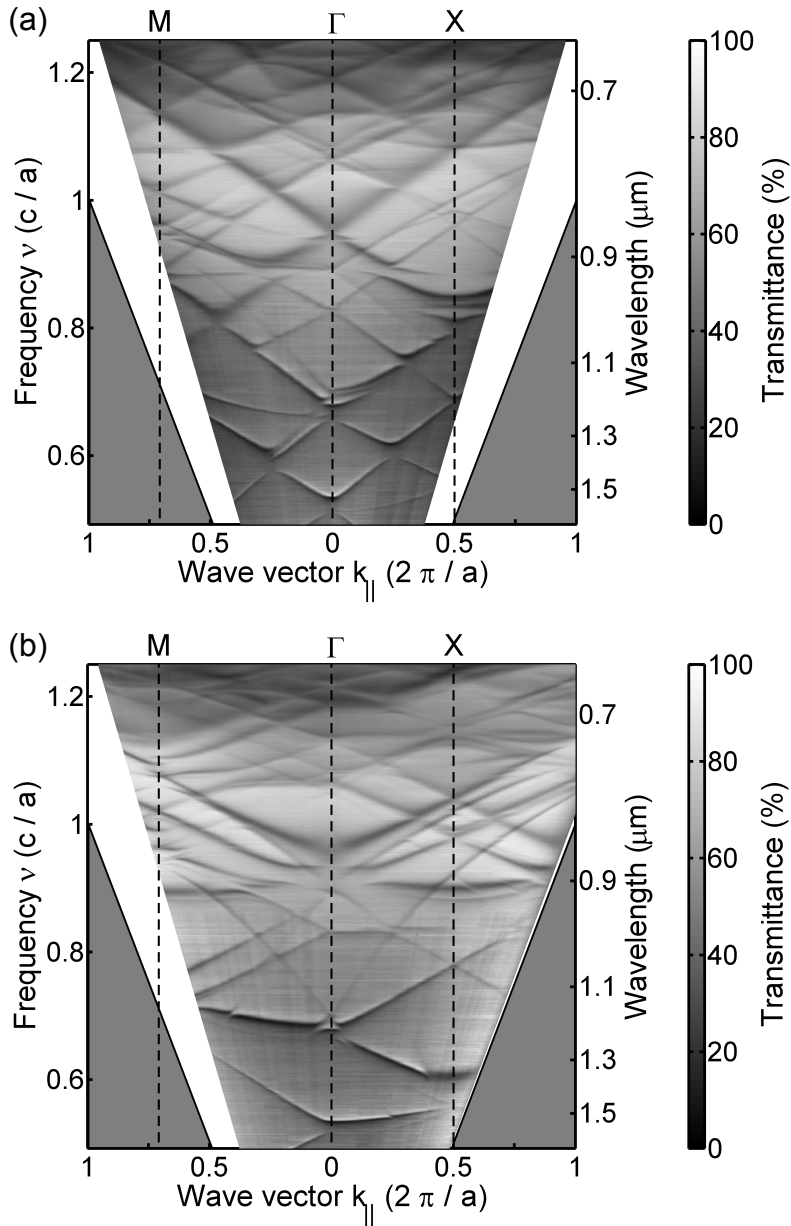


Figure 4.5. Gray scale plot of the measured transmission as a function of frequency (vertical axis) and wave vector $k_{||}$ (horizontal axis). Measurements are shown for s - (a) and p -polarized (b) incident light, and for the ΓX and the ΓM symmetry direction of the square lattice. The graphs reveal the presence of many leaky modes. The gray shaded area below the light line (solid line) is inaccessible in our experiment.

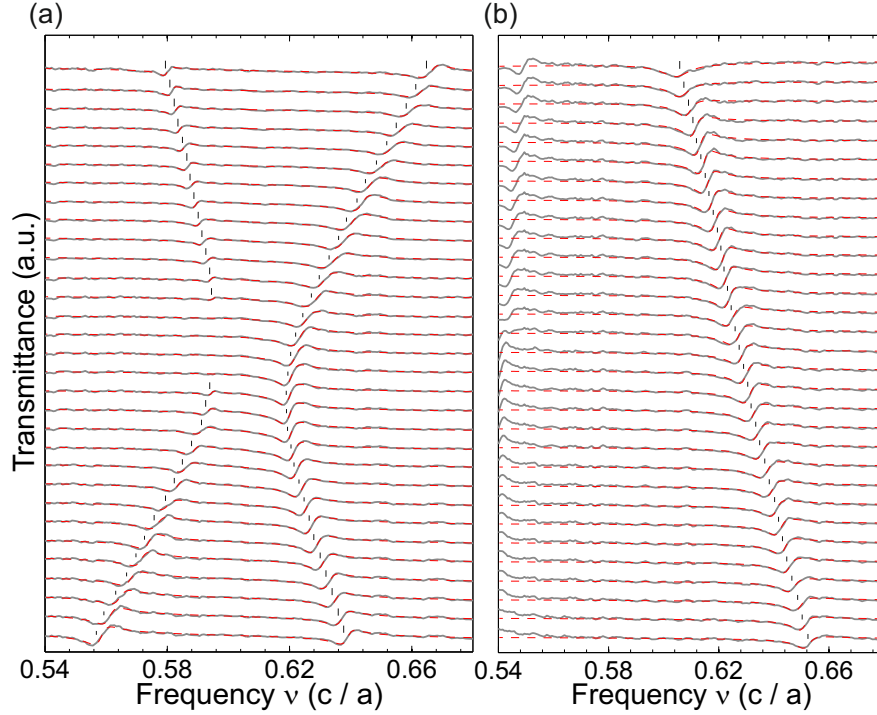


Figure 4.6. Measured transmission spectra (solid gray lines) for angles of incidence from 10° to 40° in steps of 1° , vertically offset for clarity. The experimental data are shown for wave vector k_{\parallel} along the ΓX symmetry direction and for s - (a) and p -polarization (b). The resonant features in transmission that correspond to $(1,0)$ and $(-1,\pm 1)$ modes, are fitted with Fano lineshapes (dashed red lines). Indicating the position of the resonant frequencies, the black lines serve as guides to the eye, and demonstrate the avoided crossing between the s -polarized $(1,0)$ and $(-1,\pm 1)$ mode.

between the s -polarized $(1,0)$ and $(-1,\pm 1)$ modes.

The dashed red lines are fits to the data using the Fano model. As can be seen, this model describes very well the measured transmission spectra. By fitting the Fano lineshapes to the sharp features in the spectra, we obtain the dispersion relations and the quality factors of the leaky modes. The black lines indicate the fitted center frequencies, and serve to guide the eye. At the avoided crossing, the quality factor of the lower energy $(1,0)$ mode increases while its amplitude decreases. As a result, this mode becomes subradiant and disappears from the spectra.

4. Method to transfer photonic crystals to a transparent gel substrate

To gain insight and to get quantitative data for the avoided crossing of the modes, we introduce a simplified coupled mode theory that retains the essential symmetries of a complete band structure calculation. The interaction between the three modes can be described by a coupled mode theory featuring a 3×3 matrix of the following form:

$$H = \begin{pmatrix} \nu_1 & \kappa_1 & -\kappa_1 \\ \kappa_1 & \nu_2 + \kappa_2 & \kappa_2 \\ -\kappa_1 & \kappa_2 & \nu_2 + \kappa_2 \end{pmatrix}. \quad (4.2)$$

Here ν_1 and ν_2 are the frequencies of the unperturbed modes, that is the guided modes of a dielectric slab with an appropriate effective refractive index, without holes. The symmetry and the interaction between the three modes represented by this matrix is consistent with the nearly free photon picture introduced by Sakoda et al. [82]. The dispersion of these modes, $\nu(k_{\parallel})$, can be obtained by folding the dispersion of the fundamental TE waveguide mode of the slab back to the first Brillouin zone by adding an appropriate reciprocal lattice vector. In this picture, ν_1 corresponds to the non-degenerate (1,0) mode, while ν_2 corresponds to the twofold degenerate $(-1, \pm 1)$ modes. The coupling constant κ_1 characterizes the interaction between the s -polarized (1,0) and $(-1, \pm 1)$ mode, while the coupling constant κ_2 characterizes the interaction between the two $(-1, \pm 1)$ modes.

The resonant frequencies of the leaky modes are given by the eigenvalues of the matrix H , and can be written as:

$$\nu_0 = \nu_2 + 2\kappa_2 \quad (4.3)$$

$$\nu_{\pm} = \frac{\nu_1 + \nu_2}{2} \pm \sqrt{\left(\frac{\nu_1 - \nu_2}{2}\right)^2 + 2\kappa_1^2}, \quad (4.4)$$

where ν_0 is the resonant frequency of the p -polarized $(-1, \pm 1)$ mode, ν_+ is the resonant frequency of the s -polarized $(-1, \pm 1)$ mode, and ν_- is the resonant frequency of the s -polarized (1,0) mode. The coupling between the s -polarized (1,0) and $(-1, \pm 1)$ leaky mode, introduces the frequency splitting between the two modes equal to $2\sqrt{2}\kappa_1$ at $k_{\parallel} = G/4$ ($G = 2\pi/a$).

Figure 4.7 shows the dispersion relations for the three modes obtained from the Fano fits of Fig. 4.6 (circles). The dashed lines represent the dispersion of the modes ν_1 , ν_2 in the coupled mode theory. The resulting fit of the coupled mode theory to the experimental data is represented by the solid line and shows excellent agreement. The fitted values of the coupling constants are $\kappa_1 = 0.012 \times c/a$ and $\kappa_2 = 0.022 \times c/a$. This corresponds to a splitting

relative to the center frequency of the two uncoupled modes ($\nu_c = 0.608 \times c/a$) of $2\sqrt{2}\kappa_1/\nu_c = 5.6\%$ and $2\kappa_2/\nu_c = 7.2\%$. To reduce the number of fitting parameters, we assumed that both coupling constants are independent of the in-plane wave vector k_{\parallel} .

In the coupled mode theory the uncoupled s -polarized $(1,0)$ and $(-1, \pm 1)$ leaky modes follow dispersions of $\nu_1(k_{\parallel})$ and $\nu_2(k_{\parallel})$:

$$\nu_1(k_{\parallel}) = \frac{1}{2\pi} \left((v_p - v_g) \frac{5G}{4} + v_g (k_{\parallel} + G) \right), \quad (4.5)$$

$$\nu_2(k_{\parallel}) = \frac{1}{2\pi} \left((v_p - v_g) \frac{5G}{4} + v_g \sqrt{(k_{\parallel} - G)^2 + G^2} \right), \quad (4.6)$$

where the phase velocity and group velocity are defined as

$$v_p = 2\pi \left. \frac{\nu_w}{\beta_w} \right|_{\beta_w = \beta_{w0}}, \quad (4.7)$$

$$v_g = 2\pi \left. \frac{\partial \nu_w}{\partial \beta_w} \right|_{\beta_w = \beta_{w0}}. \quad (4.8)$$

Here the dispersion relation of the waveguide mode $\nu_w(\beta_w)$ is expanded in Taylor series around the point of the avoided crossing ($\beta_{w0} = 5/4 \times 2\pi/a$, ν_{w0}), and then folded back to the first Brillouin zone. From the fit we obtain the values for the phase velocity $v_p = 0.486 \times c$ and for the group velocity $v_g = 0.327 \times c$, where c is the speed of light in vacuum. Furthermore, from the phase velocity, we determine the value of the effective refractive index of the waveguide mode $n_{w0} = 2.06$. This value is consistent with the nearly free photon picture where the effective refractive index of the guided mode n_w is limited by the refractive index of the surrounding medium $n_{gel} = 1.4$ on one side and the effective refractive index of the slab waveguide $n_{slab} \sim 3$ on the other side.

We will now discuss the quality factors of the coupled modes and the coupling to the external radiation. Only one of the $(-1, \pm 1)$ modes couples to p -polarized light, while the two other modes couple to s -polarized light. The reciprocal lattice vector $(0, 2)$ couples the two degenerate $(-1, \pm 1)$ waves with electric fields \mathbf{E}_1 and \mathbf{E}_2 ($|\mathbf{E}_1| = |\mathbf{E}_2|$), and creates two non-degenerate modes $\mathbf{E}_1 \pm \mathbf{E}_2$. The resulting mode denoted by the “+” sign has an electric field distribution which is even with respect to the mirror plane through the holes, and therefore couples to p -polarized radiation. The mode denoted by the “-” sign has an odd field distribution with respect to the same mirror plane and couples to s -polarized light. The standing wave component of the

4. Method to transfer photonic crystals to a transparent gel substrate

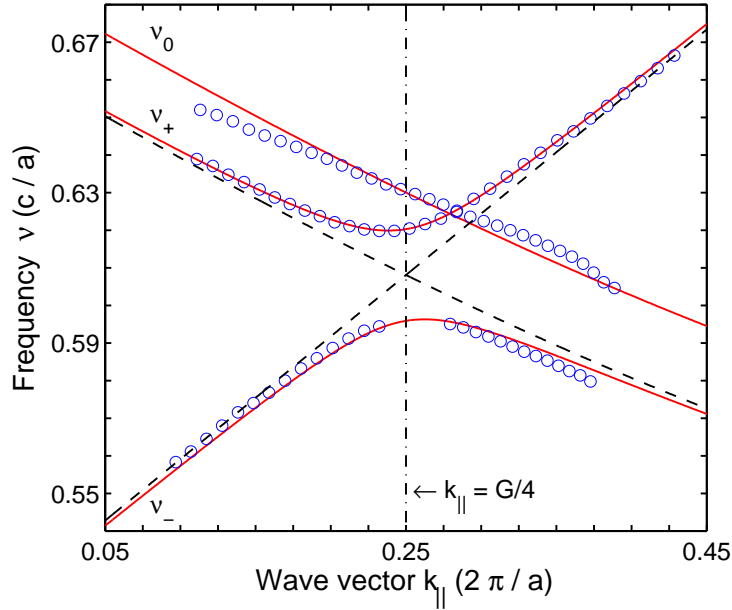


Figure 4.7. Dispersion relations for the s -polarized $(1,0)$ mode and both the s - and p -polarized $(-1,\pm 1)$ modes derived from the fits of Fig. 4.6 (circles). The solid lines are obtained from a coupled mode theory with only 3 modes (see text). Note that the labels ν_0 , ν_+ , and ν_- correspond to the p -polarized $(-1,\pm 1)$ mode, the s -polarized $(-1,\pm 1)$ mode, and the s -polarized $(1,0)$ mode, respectively. The dashed lines indicate the unperturbed modes and cross at $k_{||} = G/4$.

pattern concentrates the electric field in the holes for the p -polarized $(-1,\pm 1)$ mode, and in the dielectric medium for the s -polarized mode. As a result, the p -polarized mode is higher in frequency than the s -polarized mode [68].

The reciprocal lattice vector $(2,1)$ couples the $(1,0)$ wave with the two $(-1,\pm 1)$ waves. The two modes show an avoided crossing where one of the modes becomes long-lived (subradiant) and disappears from the spectra, while the other one becomes short-lived (superradiant) and remains visible in the spectra [83–85]. This is a feature of the external coupling that can occur in open systems where the modes are coupled via a continuum [86, 87]. The radiation of one mode into the surroundings is suppressed by destructive interference, and as a result the quality factor of this mode is considerably increased. Meanwhile, the radiation of the other mode into the continuum is increased via constructive interference and the corresponding quality factor is decreased.

Figure 4.8 shows the quality factor (Q) for the s -polarized (1,0) mode as a function of the wave vector k_{\parallel} oriented along the ΓX symmetry direction (blue circles), as obtained by fitting a Fano model to the experimental transmission spectra. The error bars represent 95% confidence intervals determined from the fit. The dashed red line is a prediction of the quality factor and is given by

$$\frac{1}{Q} = \frac{1}{Q_{ideal}} + \frac{1}{Q_{loss}}. \quad (4.9)$$

Here Q_{ideal} is the calculated quality factor of the s -polarized (1,0) leaky mode for an ideal two-dimensional photonic crystal slab with parameters identical to the experimental structure. In experimental structures this quality factor is never reached due to absorption, imperfections and/or finite size effects. The effect of these loss mechanisms is characterized with the quality factor Q_{loss} .

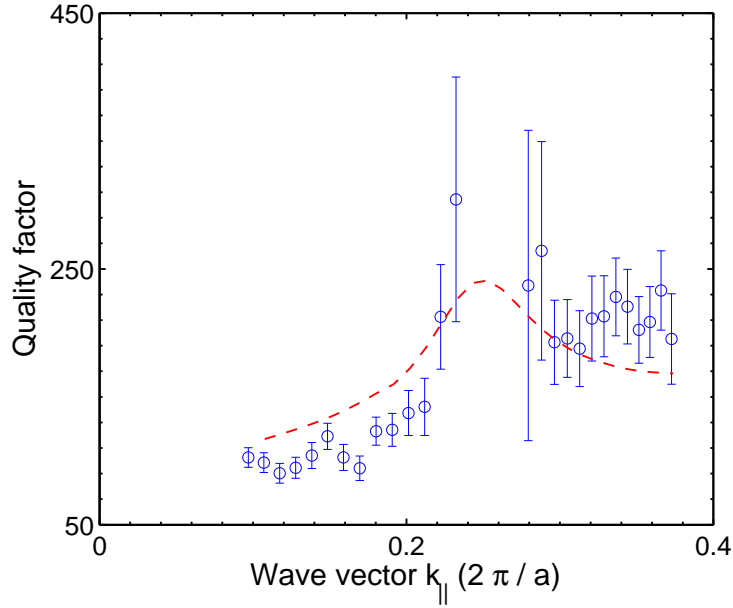


Figure 4.8. Experimental quality (Q) factor (blue circles) of the (1,0) mode as a function of the wave vector k_{\parallel} , obtained by fitting the Fano model to the measured transmission spectra. Error bars represent 95% confidence intervals determined from the fit. The calculated quality factor for an ideal two-dimensional photonic crystal slab is used to obtain the dashed red line which serves as a guide to the eye (see text). Quality factors as high as 300 are measured, a value limited by the finite size of the structure.

4. Method to transfer photonic crystals to a transparent gel substrate

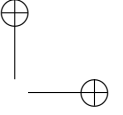
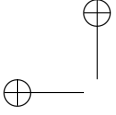
We did not attempt to accurately describe the losses in the experimental structure, and used a constant value of 250 for Q_{loss} , independent of $k_{||}$. Since the field distribution in the slab depends on the mode and $k_{||}$, it is more realistic to consider Q_{loss} as a function of $k_{||}$. In fact, the data points for $k_{||} < G/4$ ((1,0) mode) are described better with $Q_{loss} = 175$, while the data points for $k_{||} > G/4$ are described better with $Q_{loss} = 325$.

As can be seen in the figure, the quality factor increases as the wave vector $k_{||}$ approaches midway between the Γ and the X point, where the avoided crossing occurs. At the avoided crossing, the (1,0) mode disappears and the corresponding quality factor diverges. The highest measured quality factor in our case is 300. For this case, the light travels a distance of $Q\lambda_0/n_{eff} \approx 200 \mu\text{m}$ before diffracting into the surrounding media. Here $\lambda_0 = 1.38 \mu\text{m}$ and $n_{eff} = 2.06$ are the resonant wavelength and the effective refractive index of the leaky mode, respectively. Since our sample covers an area of $\sim 300 \times 300 \mu\text{m}^2$, this suggests that the quality factor is limited by the finite size of the sample, and not by the optical quality of the structure.

4.5 Conclusions

We have demonstrated a novel method to transfer large freestanding photonic crystal slabs $\sim 300 \times 300 \mu\text{m}^2$ to a transparent substrate (gel) with a low refractive index of $n_{gel} = 1.4$. This eliminates the buckling of the membranes due to a lattice mismatch between the $\text{Al}_{0.35}\text{Ga}_{0.65}\text{As}$ membrane and the GaAs substrate. As a result, almost perfectly flat membranes which allow for both the reflection and transmission measurements, are created. After the transfer to the gel, the measured resonant frequencies of the leaky modes are red shifted with respect to those of a freestanding slab. This can be explained by the change in the effective refractive index of the leaky modes via a change in dielectric environment. More importantly, the resonant features in the experimental reflection spectra for photonic crystal slabs on the gel substrate are more prominent than those for freestanding photonic crystal slabs. We believe that this is due to the removal of the Fabry-Perot cavity that is formed by the highly-reflective GaAs substrate and the wavy membrane. Therefore, the structures on the gel are more attractive for studying the resonant effects in photonic crystal slabs.

We show that the interaction between the s -polarized (1,0) and (-1, \pm 1) mode leads to an avoided crossing for the in-plane wave vector $k_{||}$ midway between the Γ and the X point of the square lattice. This avoided crossing can be described by a coupled mode theory featuring a 3×3 matrix instead of

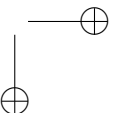
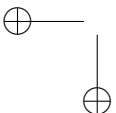


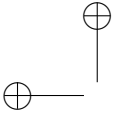
4.5 Conclusions

a complete photonic band structure calculation. At the avoided crossing the lower energy s -polarized (1,0) mode disappears from the transmission spectra becoming a subradiant mode with a high quality factor. For this mode, we measure Q factors as high as 300 and show that these values are probably limited by the finite size of our structures (diffraction) demonstrating the excellent optical quality of the transferred membranes.

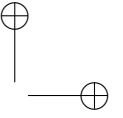
The high quality factor of leaky modes, makes our structures especially attractive for experimental study of nonlinear resonant effects, such as second harmonic generation [47–49]. Coupling to a resonance with a high Q factor accumulates considerable field intensity in the nonlinear material of a photonic crystal. If both the fundamental and the second harmonic waves couple resonantly to the structure phase-matching conditions are fulfilled [47, 48], and large enhancement in the second harmonic response can be achieved.

The presented transfer technique may prove to be a robust and relatively simple way to integrate a wide variety of devices based on different materials. The transfer technique can be applied to increase extraction efficiency of light-emitting diodes by using diffraction from a photonic crystal layer [74]. Positioning a gallium phosphide membrane with a cavity on a flat diamond substrate with nitrogen-vacancy centers to achieve long coherence times [75, 77, 78] could probably also be done with our method. Finally, it should be possible to create a versatile lab-on-chip system by picking up a high Q photonic crystal nanocavity with the gel layer, and placing it on top of a network of microfluidic channels for biochemical sensing applications. Both the photonic crystal cavity and the microfluidic channels can be fabricated independently using desired materials and technologies. This kind of freedom, intrinsic to our method, could prove to be a very useful tool for integration of photonic crystal devices in a single chip.



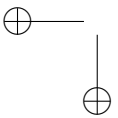


|



—

—



|

